

# Probing seismic anisotropy in North Iberia from shear wave splitting

J. Díaz<sup>a,\*</sup>, J. Gallart<sup>a</sup>, M. Ruiz<sup>a</sup>, J.A. Pulgar<sup>b</sup>, C. López-Fernández<sup>b</sup>,  
J.M. González-Cortina<sup>b</sup>

<sup>a</sup> *Department of Geophysics and Tectonics, Institute of Earth Sciences J. Almera, CSIC, Barcelona, Spain*

<sup>b</sup> *Department of Geology, University of Oviedo, Spain*

Received 29 July 2005; received in revised form 15 November 2005; accepted 20 December 2005

## Abstract

The mantle anisotropic features at the northwestern part of the Iberian Peninsula have been investigated by the shear-wave splitting technique from different temporary array deployments during the last 6 years. Successive seismic transects were instrumented from east to west, to sample areas affected by the Alpine compressional tectonics (Western Pyrenees and Cantabrian Mountains), as well as hinterland parts of the Iberian Variscan belt. A remarkable consistency is found in the retrieved anisotropic parameters throughout the study area, with an average fast velocity direction close to E/W. Delay times up to 1.5 s are observed in most transects, but lower values, not exceeding 1 s are measured at the westernmost part. Although the averaged values are compatible among the different stations, a significant variation of the splitting parameters is observed in each station with respect to the backazimuth direction. This azimuthal dependence denotes a complex distribution at depth of the anisotropic features, and cannot be explained by considering single-layer anisotropic models, either with hexagonal or orthorhombic symmetry systems, and/or dipping axes of symmetry. Synthetic models including two distinct anisotropic layers with an orthorhombic symmetry provide a satisfactory fit. In all the retained models the two layers exhibit different thicknesses; the most prominent contribution to the observed anisotropy comes from a lower layer consistently oriented close to E/W, whereas the thinner second layer, located above, ‘modulates’ the result, and its anisotropic parameters may change along the transect to account for the observed differences in splitting delay times. The dominant E–W layer throughout could not be associated to major compressional events, as in the westernmost part the Variscan terrains exhibit N–S main lineaments. It may rather correspond to an anisotropic imprint around the lithosphere–asthenosphere transition related to the eastward displacement of the Iberian plate due to the Mesozoic extensional processes during the opening of the North Atlantic and Bay of Biscay domains. The weaker anisotropic layer could be associated either with crustal anisotropic materials, or more likely, to an additional anisotropic signature within the lithosphere led by major Variscan and Alpine orogenic processes.

© 2006 Elsevier B.V. All rights reserved.

*Keywords:* Anisotropy; Shear-wave splitting; North Iberia; Lithosphere

## 1. Introduction

The presence of seismic anisotropy at some levels of the crust and upper mantle is now well established by

extensive data from permanent stations and broad-band temporary arrays covering a large variety of tectonic settings, from convergent active margins to spreading centers, collisional belts and even Archean shields (see, p.e. the compilation by Park and Levin, 2002). This feature is observed using different seismic techniques, including P-wave travel-time azimuthal variation, surface-wave scattering and shear-wave splitting, the

\* Corresponding author. Fax: +34 934 110 012.  
E-mail address: [jdiaz@ija.csic.es](mailto:jdiaz@ija.csic.es) (J. Díaz).

latter being probably the most popular tool during the last decade. The origin of the anisotropy observed at the upper crust has been related to the presence of cracks oriented at preferential directions (Crampin, 1981). The maximum delay time induced by this feature has been estimated in 0.2 s, while contributions from metamorphic rocks are also considered to be small (Barruol and Mainprice, 1993). Therefore, the main contribution to the larger anisotropy usually observed should come from upper mantle levels, where lattice preferred orientation (LPO) of the mantle minerals, in particular of olivine, is the dominant mechanism to produce anisotropy (p.e., Nicolas and Christensen, 1987), even if some anisotropy related also to LPO could exist in the lower crust (Mainprice and Nicolas, 1989). Looking for the existence of anisotropy and characterizing its geometry and amplitude could then provide the best tool to investigate the deformation of the upper mantle. However, the processes responsible for the LPO are not unique, and therefore the relationship between anisotropic results and possible deformations in the upper mantle is not straightforward. At zones with active tectonism (mid-ocean ridges, subduction zones) the anisotropic properties tend to be related to the present-day plate movement. At zones without large-scale tectonic activity, two main approaches have been developed to account for the origin of the anisotropy: those that explain the LPO as a result of dynamic flow at the lithosphere–asthenosphere limit or in the asthenospheric mantle, and those that assume an origin of the anisotropy within the lithosphere, which would preserve the structure originated by the last significant tectonic episode that affected the area. With the accumulation of new data

and the contribution of dense regional experiments, the complexity of the anisotropy has been further evidenced, and models including multiple anisotropic layers or complex symmetry systems are often required to explain the observations (see p.e. the compilation by Savage, 1999).

In this contribution we will analyze the observations on anisotropy compiled at the Northern part of the Iberian Peninsula during the last 6 years, in the framework of different Spanish research projects which have collected a large amount of passive seismic data from temporary array deployments. Major aims of these projects include local and regional seismotectonics (López-Fernández et al., 2004; Ruiz et al., 2006a,b), probing the deep structure by using receiver functions (Díaz et al., 2003), or the retrieval of anisotropic properties at some specific regions from shear-wave splitting measurements.

In a first stage, two roughly N–S transects were instrumented in the Western Pyrenees and in the eastern part of the Cantabrian Zone. In both regions the outcropping Variscan terranes have been extensively reworked on a lithospheric scale during the Alpine orogeny (Pedreira et al., 2003). First anisotropy results from those deployments were presented by Díaz et al. (2002) and will now be discussed together with those coming from the new data sets gathered in more recent deployments covering the north-westernmost part of Iberia (Fig. 1). From fall 2002 to spring 2003, portable stations were deployed westwards, along the Cantabrian Zone (CZ) and the West Asturian-Leonese Zone (WALZ), and the anisotropic reconnaissance in N Iberia was completed by another 5 months deployment in the Galicia region of the Central Iberian Zone (CIZ). These last deployments cover the hinterland Variscan domains of N Iberia where

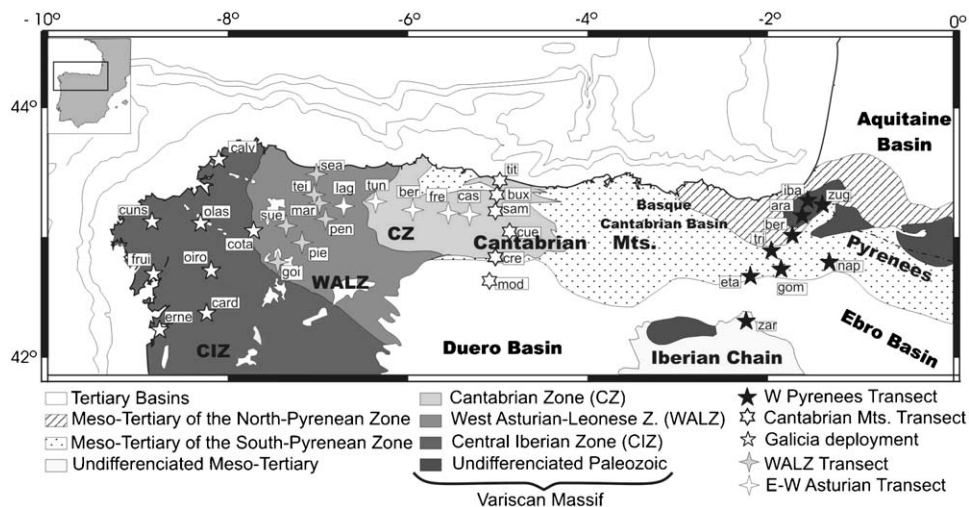


Fig. 1. Structural map of the investigated area, showing the main tectonic units and the different seismic station deployments.

there is no evidence of major Alpine rework, and where tectonic lineaments exhibit a dominant N–S direction, contrary to the mainly E–W Variscan signature on lineaments in the Cantabrian zone and the Pyrenees previously investigated. Therefore, the analysis of the whole data sets now available should reveal whether the Variscan orogeny is the major mechanism responsible for the present-day anisotropic pattern.

## 2. Tectonic setting

The Northern part of the Iberian Peninsula has suffered a complex tectonic history, being affected by the Variscan and Alpine convergences, separated by a large Mesozoic extensional episode. The Variscan orogeny started with the closure of the Rheic Ocean and the collision between Laurentia and the continental margin of Gondwana at the end of the Carboniferous (Matte, 1986, 1991), which contributed to the building of Pangea. The geological trends of this orogen show an arched pattern (Ibero-Armorican arch) with an overall E-verging structure, from the hinterland areas in the West (Iberian Massif) to the most external unit, the Cantabrian Zone to the East (Julivert et al., 1980; Pérez-Estaún et al., 1988; Matte, 1991).

Later on, the area was reworked by a large extensional period related to the opening of the North Atlantic Ocean and the Bay of Biscay, that started at chron M0 (118 Ma) and continued until chron A33 (80 Ma) (Sibuet et al., 2004). The opening of the Bay of Biscay, with an approximate N–S direction, resulted in the formation of large sedimentary basins and gave rise to the individualization of Iberia as a subplate. Most of the Cretaceous continental extension took place in a regional transtensional regime related to the left-lateral drift of the Iberian Peninsula with respect to Eurasia (Olivet, 1996; Rosenbaum et al., 2002; Srivastava et al., 1990). The opening of the North Atlantic Ocean resulted in a relative plate motion of Eurasia relative to North America oriented N108E, with a velocity of 2.2 cm/year.

Finally, the Alpine orogeny, as a result of the convergence between Iberia and Eurasia built up the doubly vergent Pyrenean–Cantabrian mountain belt and produced a displacement in the plate boundary, which jumped to the North Spanish Trough. The deformation was not coeval, beginning in the Late Cretaceous at the eastern Pyrenees (Vergés et al., 1995). The onset of deformation in the Cantabrian continental margin started on mid to Late Eocene and the present Cantabrian Mountains developed in Eocene to Miocene times (Gallastegui et al., 2002). The involved shortening has been evaluated between 150 km in central Pyrenees (Choukroune, 1989;

Muñoz, 1992) to 75 km in the west central Pyrenees (Séguret and Daignières, 1986; Teixell, 1998), while in the Cantabrian Mountains and continental margin net shortening reaches almost 100 km (Gallastegui et al., 2002; Pedreira et al., 2003).

The main structural units in the western end of the Pyrenean Chain are the Paleozoic Massifs of the axial zone, located in the central part and bordered by the North and South Pyrenean zones, corresponding to Mesozoic and Cenozoic units overthrusting the Tertiary Aquitaine and Ebro foreland basins (Fig. 1). Moving to the West, the Cantabrian Mountains are constituted by two zones: the Basque–Cantabrian Basin, an inverted large Mesozoic basin resulting from extensional regime associated to the opening of the Bay of Biscay, and the Asturian Massif, which represents a Paleozoic basement block uplifted along a major basement thrust (Alonso et al., 1996).

The Iberian Variscan Belt in NW Spain constitutes an ancient continental margin involved in the Variscan collision (Matte, 1986, 1991), with a well established zonation, based on structural, metamorphic and paleogeographic differences, between the foreland in the East to the hinterland areas in the West (Julivert et al., 1972; Fariás et al., 1987). The Cantabrian Zone corresponds to the foreland thrust and fold belt of the Variscan chain and is characterized by thin-skinned tectonics and a rather tight arcuate trend (Pérez-Estaún et al., 1988, 1994). The hinterland zones are located immediately westwards, and its first unit is the WALZ, interpreted as a transitional area, with westward increasing metamorphism and internal deformation (Martínez Catalán et al., 1990). Finally, the western end of northern Iberia is covered by the Central Iberian Zone, corresponding to the most internal units of the Variscan orogeny (Fig. 1).

## 3. Data acquisition and anisotropic parameters retrieval

Here, we analyze data from different acquisition experiments carried out in the northern part of Iberia between 1999 and 2003 (Fig. 1). The first deployment (referred from now on as WPyr) samples a N–S/NE–SW transect at the western end of the Pyrenees, extending from the wedge of the Iberian Chain to the axial zone of the Pyrenees, and was operational during a total of 15 months in two different periods. The second deployment delineates a N–S transect along the eastern part of the Cantabrian Zone (ECZ), and was active during a 9 month period. These two transects were instrumented using six seismic stations equipped with Lennartz seismometers (Le20s and Le5s), with flat velocity response

Table 1  
Location of the events retained in this study

Deployment <sup>a</sup>	Event	Year	Julian day	Time	Latitude	Longitude	Depth	Magnitude
ECZ	Taiw263	1999	263	17:47:19	23.78	121.09	33	7.6
ECZ	Taiw268	1999	268	23:52:51	23.78	121.12	33	6.5
ECZ	Indi319	1999	319	05:42:43	-1.42	89.00	10	7.0
ECZ	NBri323	1999	323	13:56:46	-6.43	148.67	33	5.9
ECZ	Luzo345	1999	345	18:03:36	15.80	119.76	33	6.8
ECZ	Kuri028	2000	28	14:21:07	43.06	146.81	62	6.8
ECZ	Nbri037	2000	37	11:33:52	-5.86	150.83	33	6.7
ECZ	WChi075	2000	75	06:35:05	-44.29	-117.27	10	5.9
ECZ	Volc088	2000	88	11:00:20	22.41	143.59	116	7.7
ECZ	Este114	2000	114	09:27:22	-28.25	-62.89	603	6.9
ECZ	Minal25	2000	125	04:21:17	-0.90	123.4	33	7.3
ECZ	Suma156	2000	156	16:28:25	-4.73	102.05	33	7.9
ECZ	Chil169	2000	169	07:55:35	-33.89	-70.00	119	6.4
ECZ	Boni219	2000	219	07:27:18	28.89	139.46	452	7.3
W_Pyr	Sund299	2000	299	09:32:22	-6.66	105.55	33	6.8
W_Pyr	Boni301	2000	301	04:21:51	26.28	140.52	383	6.1
W_Pyr	Nire321	2000	321	07:42:16	-5.24	153.06	33	8.0
W_Pyr	NBri323	2000	323	06:54:59	-5.20	151.68	33	6.6
W_Pyr	NBri341	2000	341	22:57:40	-4.17	152.81	33	6.6
W_Pyr	Vanu009	2001	9	16:49:28	-14.85	167.05	104	6.9
W_Pyr	Molu055	2001	55	07:23:48	1.46	126.3	33	7.0
W_Pyr	Hons083	2001	83	06:27:52	34.13	132.56	33	6.5
W_Pyr	Hokk116	2001	116	17:48:57	43.23	145.75	82	5.9
W_Pyr	Fidj118	2001	118	04:49:52	-18.01	-177.00	351	6.7
W_Pyr	Jawa145	2001	145	05:05:59	-7.91	110.26	33	5.9
W_Pyr	Solo149	2001	149	23:37:22	-7.02	154.94	33	6.4
W_Pyr	Kerm154	2001	154	02:41:58	-29.47	-178.59	183	7.1
W_Pyr	NGui156	2001	156	09:00:04	-6.89	146.57	10	6.4
W_Pyr	Taiw165	2001	165	02:35:25	24.49	121.97	33	5.9
WALZ-EW_Ast	Chil169	2002	169	13:56:22	-30.78	-70.93	52	6.5
WALZ-EW_Ast	Rusi179	2002	179	17:19:30	43.77	130.72	564	7.3
WALZ-EW_Ast	Fiji181	2002	181	21:29:36	-22.18	179.20	619	6.5
WALZ-EW_Ast	Caro226	2002	226	13:12:39	7.81	136.85	10	6.2
WALZ-EW_Ast	Fiji231	2002	231	11:08:25	-23.85	178.41	694	7.7
WALZ-EW_Ast	NGui251	2002	251	18:44:26	-3.24	142.89	33	7.6
WALZ-EW_Ast	Rusi258	2002	258	08:39:31	44.86	130.08	578	6.5
WALZ-EW_Ast	NGui259	2002	259	13:23:00	-3.28	142.62	10	6.3
WALZ-EW_Ast	NGui260	2002	260	11:20:23	-3.25	142.79	10	6.1
WALZ-EW_Ast	Suma306	2002	306	01:26:11	3.02	96.18	33	7.5
WALZ-EW_Ast	Kuri321	2002	321	04:53:51	47.98	146.29	507	7.5
WALZ-EW_Ast	Admi354	2002	354	14:14:41	-2.94	147.67	33	6.3
WALZ-EW_Ast	Nire010	2003	10	13:11:56	-5.23	153.55	71	6.7
CIZ	Hons146	2003	146	09:24:33	38.89	141.51	69	7.0
CIZ	Mind146	2003	146	23:13:29	6.80	123.75	559	6.8
CIZ	NBri158	2003	158	00:32:45	-5.10	152.40	33	6.7
CIZ	Rat1174	2003	174	12:12:36	51.60	176.68	37	6.9
CIZ	NBri185	2003	185	00:33:53	-5.48	151.66	33	5.9
CIZ	Nire206	2003	206	09:37:48	-1.49	149.63	41	6.3
CIZ	Prim208	2003	208	06:25:31	47.18	139.21	462	6.7
CIZ	Scot216	2003	216	04:37:20	-60.56	-43.49	10	7.5
CIZ	Anda223	2003	223	21:22:30	12.14	93.52	101	5.9

<sup>a</sup> ECZ: East Cantabrian Zone; W\_Pyr: Western Pyrenees; WALZ: West Asturian-Leonese Zone; EW\_Ast: East-West Asturias; CIZ: Central Iberian Zone.

electronically broadened up to periods of 20 and 5 s, respectively.

In a later experiment, two additional transects were deployed, one of them along a N–S transect located at the West Asturian-Leonese Zone (NS-WALZ), and the second along an E–W profile connecting the WALZ and the ECZ transects (EW-Ast). In this case a total of 12 stations, all of them equipped with Le20s seismometers, were installed for a period of about 9 months between summer 2002 and spring 2003. Finally, the Central Iberian Zone (CIZ) at the NW edge of Iberia was investigated by a network of eight stations with Le20s seismometers over the Galicia region for a period of 5 months during summer 2003.

In all cases, data were recorded continuously at a rate of 50 samples per second. Teleseismic events with reported magnitudes 5.5 or higher were inspected visually to identify high-quality shear wave signals, includ-

ing SKS, SKKS and PKS phases. The data were filtered before analysis using a zero-phase band-pass with typical band-pass frequency ranges of 0.01–0.2 Hz. Only events with good signal-to-noise ratio, clear phase identification and signal-to-noise ratio higher than 3 have been retained (Table 1).

In a first step, the data were interpreted assuming the usual hypothesis of waves propagating across a single layer of anisotropic material with hexagonal symmetry and horizontal symmetry axis, located over an isotropic half-space. The presence of anisotropy in the zone sampled by the ray will produce the splitting of the incoming shear wave into two orthogonally polarized waves separated by a time delay ( $\delta t$ ), resulting in the observation of elliptical polarization at the horizontal plane. Therefore, the observation of such polarization is interpreted as evidence of anisotropy and the observed  $\delta t$  provides a measure of the anisotropy degree. The use of SKS,

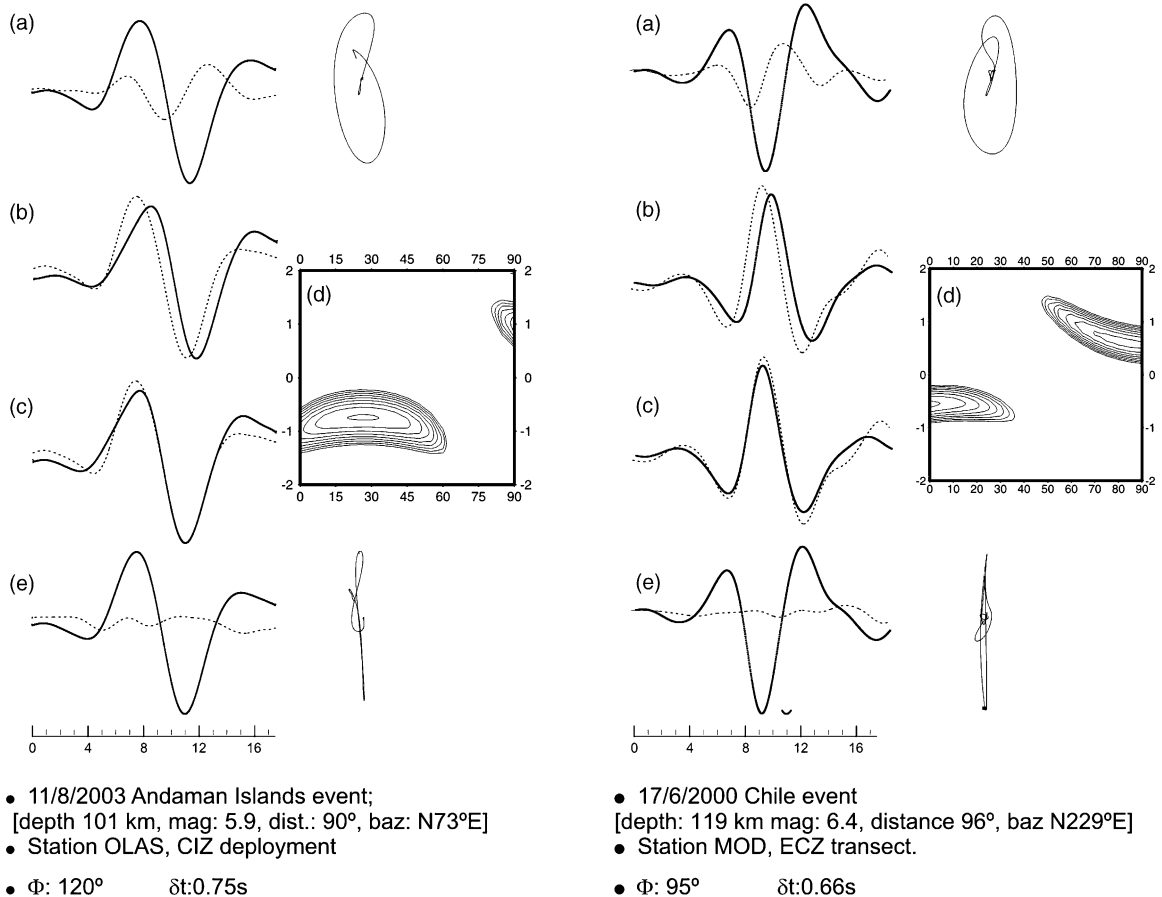


Fig. 2. Two examples of splitting measurements. For each case: (a) radial (solid line) and tangential (dashed line) components and the particle motion diagram, (b) projection to the defined fast (dashed line) and slow (solid line) directions, (c) idem, after removal of the anisotropic effect and (d) variation of the correlation coefficient with backazimuth and  $\delta t$ . (e) Radial and tangential components and the particle motion diagram after removal of the anisotropic effect.

Table 2  
Anisotropic measurements retained

Deployment	Event	Station	BAZ	Distance	$\phi$	$\delta t$	Wave	Quality
W Pyrenees	hokk116	ara	23	90	70	0.60	skks	f
W Pyrenees	boni301	ara	34	103	80	0.62	skks	f
W Pyrenees	hons083	ara	36	92	80	1.28	skks	f
W Pyrenees	nbri341	ara	38	135	70	0.88	pks	f
W Pyrenees	ngui156	ara	47	135	95	0.54	pks	g
W Pyrenees	jawa145	ara	80	111	135	0.52	skks	g
W Pyrenees	sund299	ara	82	107	125	0.80	skks	p
W Pyrenees	kerma154	ara	348	166	115	1.54	skks	f
W Pyrenees	solo149	ber	36	138	70	0.66	pks	f
W Pyrenees	ngui156	ber	47	135	85	0.48	pks	g
W Pyrenees	kerma154	ber	348	166	115	1.02	skks	f
W Pyrenees	kerma154	ber	348	166	110	1.10	skks	f
W Pyrenees	fiji118	ber	350	155	110	0.5	skks	g
W Pyrenees	vanu009	gom	22	150	50	0.86	skks	f
W Pyrenees	hokk116	gom	23	90	65	0.70	skks	g
W Pyrenees	boni301	gom	34	103	80	0.84	skks	f
W Pyrenees	solo149	gom	36	138	80	0.40	pks	f
W Pyrenees	ngui156	gom	47	135	100	0.86	pks	g
W Pyrenees	ngui156	gom	47	135	80	1.10	skks	g
W Pyrenees	fiji118	gom	350	155	130	0.74	skks	g
W Pyrenees	hons083	nap	36	92	65	0.88	skks	f
W Pyrenees	nire321	nap	39	136	70	1.00	skks	f
W Pyrenees	ngui156	nap	47	135	100	0.40	pks	g
W Pyrenees	molu055	nap	61	116	95	0.89	skks	f
W Pyrenees	kerma154	nap	348	166	90	1.24	skks	f
W Pyrenees	fiji118	nap	350	155	95	1.30	skks	f
W Pyrenees	vanu009	zar	22	150	75	0.80	skks	g
W Pyrenees	vanu009	zar	22	150	80	1.44	skks	f
W Pyrenees	hokk116	zar	23	90	75	0.80	skks	g
W Pyrenees	boni301	zar	34	103	90	0.96	skks	g
W Pyrenees	hons083	zar	36	92	95	1.20	skks	f
W Pyrenees	solo149	zar	36	138	75	0.76	pks	g
W Pyrenees	nbri323	zar	40	136	80	0.84	pks	g
W Pyrenees	ngui156	zar	47	135	100	0.58	pks	g
W Pyrenees	taiw165	zar	50	96	75	1.20	skks	g
W Pyrenees	jawa145	zar	80	111	130	0.50	skks	g
W Pyrenees	jawa145	zar	80	111	140	0.70	skks	g
W Pyrenees	sund299	zar	82	107	150	0.80	skks	f
W Pyrenees	kerma154	zar	348	166	105	1.32	skks	g
W Pyrenees	fiji118	zar	350	155	135	1.30	skks	g
W Pyrenees	solo149	zug	36	138	65	0.60	pks	f
W Pyrenees	nbri323	zug	40	136	80	0.64	pks	f
W Pyrenees	ngui156	zug	47	135	95	0.48	pks	f
W Pyrenees	molu055	zug	61	116	100	0.96	skks	g
W Pyrenees	kerma154	zug	348	166	100	0.80	skks	f
W Pyrenees	kerma154	zug	348	166	110	1.60	skks	f
ECZ	volc088	mod	30	109	75	0.62	skks	g
ECZ	boni219	mod	31	101	75	0.60	skks	f
ECZ	minh125	mod	62	118	105	0.76	skks	g
ECZ	indi319	mod	88	94	125	0.64	skks	f
ECZ	este114	mod	228	88	90	0.70	skks	g
ECZ	chil169	mod	229	96	95	0.66	skks	g
ECZ	kuri028	cre	20	90	70	0.60	skks	g
ECZ	volc088	cre	30	109	80	0.80	skks	f
ECZ	volc088	cre	30	109	75	0.74	skks	g
ECZ	nbri037	cre	36	137	95	0.88	pks	f
ECZ	nbri037	cre	36	137	65	0.96	skks	f

Table 2 (Continued)

Deployment	Event	Station	BAZ	Distance	$\phi$	$\delta t$	Wave	Quality
ECZ	nbri323	cre	40	137	85	0.80	pks	g
ECZ	taiw263	cre	48	97	90	1.28	skks	g
ECZ	taiw268	cre	48	97	100	0.88	sks	g
ECZ	luzo345	cre	54	103	95	0.80	sks	f
ECZ	minh125	cre	62	118	105	0.86	sks	g
ECZ	indi319	cre	88	94	125	0.76	sks	g
ECZ	este114	cre	228	88	85	1.00	sks	g
ECZ	chil169	cre	229	96	95	1.06	sks	g
ECZ	kuri028	bux	20	90	65	0.50	sks	g
ECZ	volc088	bux	30	109	85	0.60	sks	g
ECZ	volc088	bux	30	109	80	0.64	skks	f
ECZ	nbri037	bux	36	137	80	0.30	pks	f
ECZ	taiw263	bux	48	97	95	0.90	skks	f
ECZ	luzo345	bux	54	103	105	0.66	sks	f
ECZ	minh125	bux	62	118	100	0.56	sks	f
ECZ	suma156	bux	82	106	120	0.64	sks	f
ECZ	este114	bux	228	88	100	0.98	sks	g
ECZ	chil169	bux	229	96	95	0.58	sks	g
ECZ	volc088	sam	30	109	85	0.40	sks	f
ECZ	volc088	sam	30	109	75	0.40	skks	g
ECZ	nbri037	sam	36	137	80	0.34	pks	f
ECZ	nbri323	sam	40	137	85	0.40	pks	f
ECZ	taiw263	sam	48	97	95	0.80	skks	g
ECZ	taiw268	sam	48	97	100	1.40	sks	g
ECZ	luzo345	sam	54	103	105	0.50	sks	g
ECZ	minh125	sam	62	118	120	0.70	sks	g
ECZ	suma156	sam	82	106	125	0.68	sks	f
ECZ	este114	sam	228	88	90	1.00	sks	g
ECZ	chil169	sam	229	96	95	0.92	sks	g
ECZ	kuri028	cue	20	90	65	0.50	sks	g
ECZ	volc088	cue	30	109	80	1.10	sks	f
ECZ	volc088	cue	30	109	80	0.74	skks	g
ECZ	boni219	cue	31	101	80	1.00	sks	g
ECZ	nbri037	cue	36	137	90	0.60	pks	g
ECZ	este114	cue	318	88	95	1.20	sks	g
ECZ	chil169	cue	319	96	95	1.40	sks	g
ECZ	volc088	tit	30	109	80	0.60	sks	g
ECZ	volc088	tit	30	109	75	0.60	skks	g
ECZ	nbri037	tit	36	137	80	0.50	pks	g
ECZ	nbri323	tit	40	137	95	0.74	pks	g
ECZ	taiw263	tit	48	97	90	1.28	skks	g
ECZ	taiw268	tit	48	97	90	0.40	sks	f
ECZ	luzo345	tit	54	103	95	0.66	sks	g
ECZ	minh125	tit	62	118	95	0.64	sks	g
ECZ	suma156	tit	82	106	130	1.20	sks	g
ECZ	este114	tit	228	88	105	1.10	sks	g
ECZ	wchi075	tit	244	132	110	0.76	pks	g
EW Asturias	kuri321	ber	17	87	60	0.00	sks	g
EW Asturias	rusi258	ber	29	85	65	0.50	sks	g
EW Asturias	rusi179	ber	30	85	70	0.80	sks	g
EW Asturias	ngui251	ber	43	131	90	0.30	pks	f
EW Asturias	ngui260	ber	44	131	90	0.30	pks	g
EW Asturias	chil169	ber	231	95	110	0.92	skks	g
EW Asturias	fiji181	ber	347	159	120	0.30	skks	f
EW Asturias	kuri321	fre	17	87	55	0.46	sks	f
EW Asturias	rusi258	fre	29	85	65	0.76	sks	f
EW Asturias	nire010	fre	32	138	90	1.00	pks	f
EW Asturias	admi354	fre	36	134	85	0.88	pks	f

Table 2 (Continued)

Deployment	Event	Station	BAZ	Distance	$\phi$	$\delta t$	Wave	Quality
EW Asturias	ngui251	fre	43	131	90	0.42	pks	g
EW Asturias	ngui259	fre	44	131	90	0.42	pks	g
EW Asturias	ngui260	fre	44	131	95	0.20	pks	g
EW Asturias	suma306	fre	80	97	150	0.40	skks	f
EW Asturias	rusi258	lag	29	85	70	0.60	sks	g
EW Asturias	rusi179	lag	30	85	75	0.84	sks	g
EW Asturias	ngui251	lag	43	131	95	0.35	pks	g
EW Asturias	chil169	lag	231	95	105	0.70	skks	g
EW Asturias	fiji181	lag	347	159	130	0.70	skks	g
EW Asturias	fiji231	lag	348	160	135	0.82	skks	g
EW Asturias	rusi258	tun	29	85	75	0.56	sks	f
EW Asturias	rusi179	tun	30	85	75	0.60	sks	f
EW Asturias	admi354	tun	36	134	75	0.00	pks	f
EW Asturias	caro226	tun	43	119	75	0.30	sks	g
EW Asturias	ngui251	tun	43	131	80	0.00	pks	f
EW Asturias	suma306	tun	80	97	140	0.44	skks	f
EW Asturias	chil169	tun	231	95	105	0.72	skks	g
EW Asturias	fiji231	tun	348	160	125	0.36	skks	g
NS-WALZ	kamc289	goi	10	84	70	0.00	sks	f
NS-WALZ	kuri321	goi	17	87	60	0.40	sks	g
NS-WALZ	rusi258	goi	29	85	65	0.50	sks	f
NS-WALZ	rusi179	goi	30	85	75	0.70	sks	g
NS-WALZ	nire010	goi	32	138	80	0.40	pks	g
NS-WALZ	admi354	goi	36	134	80	0.00	pks	f
NS-WALZ	ngui251	goi	43	131	85	0.30	pks	f
NS-WALZ	ngui259	goi	44	131	95	0.50	pks	g
NS-WALZ	ngui260	goi	44	131	80	0.60	pks	g
NS-WALZ	fiji181	goi	347	159	130	0.50	skks	g
NS-WALZ	fiji231	goi	348	160	115	0.87	skks	g
NS-WALZ	kuri321	mar	17	87	60	0.30	sks	g
NS-WALZ	rusi258	mar	29	85	70	0.74	sks	g
NS-WALZ	nire010	mar	32	138	70	0.39	pks	g
NS-WALZ	admi354	mar	36	134	85	0.73	pks	g
NS-WALZ	ngui251	mar	43	131	95	0.35	pks	g
NS-WALZ	suma306	mar	80	97	135	0.60	skks	g
NS-WALZ	fiji231	mar	348	160	140	0.80	skks	f
NS-WALZ	rusi179	pen	30	85	80	0.60	sks	f
NS-WALZ	chil169	pen	231	95	100	0.40	skks	f
NS-WALZ	fiji181	pen	347	159	125	0.60	skks	g
NS-WALZ	kuri321	pie	17	87	60	0.40	sks	g
NS-WALZ	rusi258	pie	29	85	75	0.93	sks	g
NS-WALZ	rusi179	pie	30	85	80	0.95	sks	g
NS-WALZ	ngui251	pie	43	131	95	1.08	pks	g
NS-WALZ	fiji231	pie	348	160	130	0.96	skks	g
NS-WALZ	kuri321	sea	17	87	70	0.25	sks	f
NS-WALZ	rusi258	sea	29	85	75	0.60	sks	f
NS-WALZ	caro226	sea	43	119	105	0.00	sks	f
NS-WALZ	ngui251	sea	43	131	100	0.52	pks	f
NS-WALZ	suma306	sea	80	97	135	0.60	skks	f
NS-WALZ	chil169	sea	231	95	105	1.00	skks	g
CIZ	Prim208	CARD	21	86	80	0.00	sks	g
CIZ	NBri185	CALV	31	138	65	0.35	pks	g
CIZ	RatI174	CALV	357	85	135	0.56	sks	f
CIZ	Nire206	CARD	31	134	90	0.00	pks	f
CIZ	Scot216	CARD	197	107	90	0.00	sks	f
CIZ	RatI174	CARD	356	86	145	0.85	sks	g
CIZ	Hons146	COTA	23	93	70	0.30	sks	g
CIZ	NBri158	COTA	30	138	75	0.60	pks	g

Table 2 (Continued)

Deployment	Event	Station	BAZ	Distance	$\phi$	$\delta t$	Wave	Quality
CIZ	Mind146	COTA	54	113	95	0.50	sdif	g
CIZ	Rat174	COTA	357	85	135	0.80	sks	g
CIZ	Hons146	CUNS	22	93	70	0.20	sks	g
CIZ	NBri158	CUNS	29	138	80	0.40	pks	g
CIZ	NIre206	CUNS	30	134	85	0.30	pks	f
CIZ	NBri185	CUNS	30	138	90	0.50	pks	g
CIZ	Mind146	CUNS	53	114	100	0.60	sdif	g
CIZ	Rat174	CUNS	356	85	130	0.35	sks	g
CIZ	Prim208	ERNE	21	86	70	0.00	sks	g
CIZ	Mind146	ERNE	53	114	105	0.00	sdif	p
CIZ	Scot216	ERNE	197	106	65	0.00	sks	g
CIZ	Rat174	ERNE	356	86	145	1.00	sks	g
CIZ	Prim208	GOIA	22	85	60	0.35	sks	g
CIZ	Hons146	GOIA	23	93	65	0.28	sks	g
CIZ	NBri158	GOIA	31	138	70	0.60	pks	g
CIZ	NIre206	GOIA	32	134	75	0.30	pks	g
CIZ	Mind146	GOIA	54	113	95	0.50	sdif	g
CIZ	Anda223	GOIA	73	89	115	0.50	sks	g
CIZ	Rat174	GOIA	357	85	140	0.35	sks	f
CIZ	Prim208	OIRO	21	85	60	0.35	sks	g
CIZ	Hons146	OIRO	23	94	75	0.20	sks	g
CIZ	NBri158	OIRO	30	138	85	0.50	pks	f
CIZ	NBri185	OIRO	31	138	85	0.30	pks	g
CIZ	Mind146	OIRO	54	114	110	0.35	sdif	g
CIZ	Anda223	OIRO	73	90	125	0.45	sks	g
CIZ	Prim208	OLAS	21	85	50	0.15	sks	g
CIZ	NIre206	OLAS	31	134	70	0.30	pks	g
CIZ	NBri185	OLAS	31	138	65	0.35	pks	g
CIZ	Anda223	OLAS	73	90	120	0.75	sks	g
CIZ	Rat174	OLAS	356	85	140	0.50	sks	g

For each measurement, the backazimuth, distance, fast velocity direction, delay time, phase and quality factor are showed.

SKKS and PKS waves assures that the anisotropy zone must be located beneath the receiver, as the propagation as P wave across the external core will remove the effect of possible source-side anisotropy.

If the signal is projected into the coordinate system formed by the principal axis of symmetry of the anisotropic system, the two quasi-shear waves will appear as identical wavelets, separated by a certain  $\delta t$ . Hence, to measure the anisotropic parameters, a grid search is done by projecting the horizontal components in different coordinate system orientations (every  $5^\circ$ ) and displacing them by 0.01 s time intervals. The fitting of the two horizontal waveforms is quantified in each case using their correlation coefficient. The coordinate system and delay time which provide the best adjustment defines the anisotropic parameters. Only when the transverse energy can be significantly removed, as verified in the particle motion diagrams, the measurement is retained. Examples of this procedure for two stations at the ECZ and CIZ deployments are presented at Fig. 2.

We have observed that this requirement may not be well constrained just by the correlation coefficient, because in cases of relatively noisy signals, small changes in the time interval where the signals are correlated, as well as changes in the band pass filter applied to the data, result in significant variations in the retrieved anisotropic values. Therefore, we prefer to assign a quality factor to each measurement that takes into account all these facts. The obtained measurements are qualified in three groups (poor, fair and good). However, to avoid misinterpretations due to poor quality data, only measurements qualified as ‘good’ or ‘fair’ have been retained in the subsequent analysis. ‘Good’ quality measurements are robust and their fast velocity direction uncertainties can be estimated in  $\pm 5^\circ$ . ‘Fair’ quality measurements are also well constrained during the grid search but are less robust when different band-pass filters and correlation time windows are tested. Its uncertainty may be estimated in  $\pm 10^\circ$ . This led to 15 events and 47 individual measurements in the WPyr transect, 14 events and 58

measurements in the ECZ transect, 13 events and 61 measurements in the NS-WALZ and EW-Ast transects and 9 events and 38 measurements in the CIZ deployment.

#### 4. Splitting measurement results

The measured anisotropy parameters for the different stations in all deployments are presented on Table 2. The results are summarized on Table 3, which shows the number of measurements for each station together with the mean value, standard deviation and range of variation of the fast velocity direction  $\phi$  and the induced delay time  $\delta t$ . The obtained results provide a continuous image of the anisotropic properties beneath the northern part of the Iberian Peninsula, along a major transect from the

Atlantic coast to the Pyrenean range. Main parameters for representative stations are displayed in Fig. 3.

The first-order result is a remarkable consistency of the average fast directions observed for all the stations at the different deployments. A large majority of stations have average  $\phi$  values lying between N90°E and N100°E. Concerning the induced delay times, the results are also similar, without any station exceeding an average delay time of 1.5 s. However, it should be noted that stations on the Variscan units, and in particular those deployed over the Central Iberian Zone, show mean  $\delta t$  values consistently lower than those in the ECZ and W-Pyr transects. Moreover, at some of the former stations, few good quality events show no evidence of splitting, providing ‘null’ measurements.

Table 3  
Mean  $\phi$  and  $\delta t$  values and their range of variation for all the stations

Deployment	Station	Latitude	Longitude	# Data	$\phi$	$\phi$ range	$\sigma\phi$	$\delta t$	$\delta t$ range	$\sigma\delta t$
W Pyrenees	zar	42.1820	-2.3419	14	100	75–135	27	0.9	0.5–1.4	0.3
W Pyrenees	ara	43.1797	-1.7289	8	96	70–135	26	0.8	0.5–1.5	0.4
W Pyrenees	ber	43.0111	-1.8396	5	98	70–110	20	0.8	0.5–1.1	0.3
W Pyrenees	nap	42.7129	-1.2071	6	86	65–100	15	1.0	0.4–1.3	0.3
W Pyrenees	gom	42.7066	-1.8045	7	84	50–130	26	0.8	0.4–1.1	0.2
W Pyrenees	zug	43.2493	-1.5561	6	98	65–110	16	0.8	0.6–1.6	0.4
ECZ	tit	43.4593	-5.0741	11	95	75–130	16	0.8	0.4–1.3	0.3
ECZ	bux	43.3585	-5.0999	10	92	65–120	15	0.6	0.3–1.0	0.2
ECZ	sam	43.2645	-5.1238	11	96	80–125	16	0.7	0.4–0.9	0.3
ECZ	cue	43.0631	-4.9889	7	84	65–95	11	0.9	0.5–1.4	0.3
ECZ	cre	42.9082	-5.1596	13	90	65–125	16	0.9	0.6–1.3	0.2
ECZ	mod	42.7600	-5.1528	6	94	75–125	19	0.7	0.6–0.8	0.1
NS-WALZ	goi	42.8157	-7.4696	9 + 2 <sup>a</sup>	87	60–130	23	0.5	0.3–0.9	0.2
NS-WALZ	mar	43.2741	-7.0040	7	94	60–140	32	0.6	0.3–0.8	0.2
NS-WALZ	pen	43.1479	-6.9338	3	102	80–125	23	0.5	0.4–0.6	0.1
NS-WALZ	pie	42.9596	-7.2080	5	88	60–130	27	0.9	0.4–1.0	0.3
NS-WALZ	sea	43.4845	-7.0282	5 + 1 <sup>a</sup>	97	70–125	26	0.6	0.2–1.0	0.3
EW-Asturias	ber	43.2200	-5.9728	6 + 1 <sup>a</sup>	91	65–120	22	0.5	0.3–0.9	0.3
EW-Asturias	fre	43.1994	-5.5763	8	90	55–150	28	0.6	0.2–1.0	0.3
EW-Asturias	lag	43.2531	-6.7306	6	102	70–135	27	0.7	0.3–0.8	0.2
EW-Asturias	tun	43.2738	-6.3794	6 + 2 <sup>a</sup>	99	75–140	29	0.5	0.3–0.7	0.2
CIZ	CALV	43.6111	-8.1010	2	100	65–135	49	0.5	0.3–0.5	0.1
CIZ	COTA	43.0454	-7.7207	4	94	70–135	30	0.5	0.3–0.8	0.2
CIZ	CUNS	43.1297	-8.8419	6	93	70–130	21	0.4	0.2–0.6	0.1
CIZ	GOIA	42.8157	-7.4696	7	89	60–140	30	0.4	0.3–0.6	0.1
CIZ	OIRO	42.7619	-8.1876	6	90	60–125	24	0.4	0.2–0.5	0.1
CIZ	OLAS	43.1055	-8.3093	5	89	50–140	39	0.4	0.1–0.7	0.2
Summary					$\phi$					$\delta t$
W Pyrenees					93					0.8
ECZ					93					0.7
NS-WALZ					91					0.5
EW-Asturian					95					0.6
CIZ					92					0.4

<sup>a</sup> M + N; M: non-null measurements; N: null measurements.

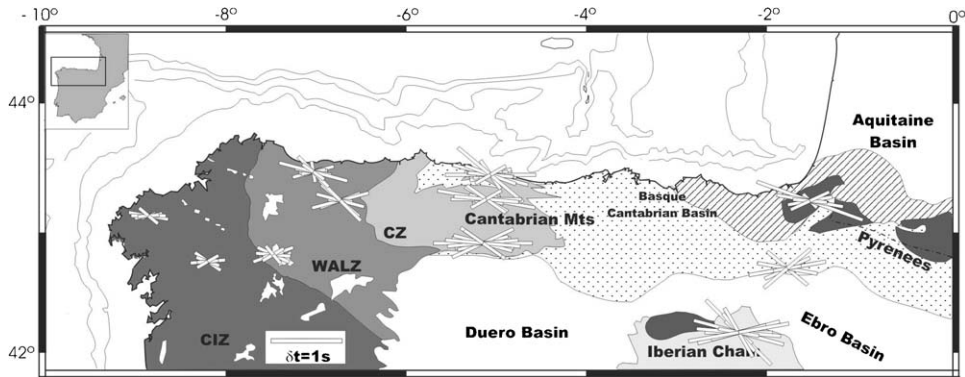


Fig. 3. Anisotropic parameters for representative stations along the different deployments over a structural map. The arrow lengths are proportional to the time delay. Refer to Fig. 1 for fill patterns.

Another important observation is the significant spread in the fast velocity directions for different events in each station, with standard deviations reaching more than  $20^\circ$  in many sites. The range of variation of the measured  $\phi$  at a single station is usually as large as  $50\text{--}70^\circ$  and cannot be justified by uncertainties within the interpretation procedure, as illustrated by the example of Fig. 4. Upper panels show the appropriate fitting obtained in the projections to the fast and slow directions when using the values determined for two different

events recorded by the same station. Lower panels show, for each event, the effect of using the anisotropic parameters inferred for the other event: in this case the fitting becomes quite poor. The mean  $\delta t$  also shows a significant spread, ranging from few tens of a second to 1.5 s for the W-Pyr and ECZ transects and up to 1.0 s for the Variscan units.

We have then investigated whether this spread shows any systematic azimuthal dependence. We plotted  $\phi$  and  $\delta t$  as a function of the backazimuth of the events and, as

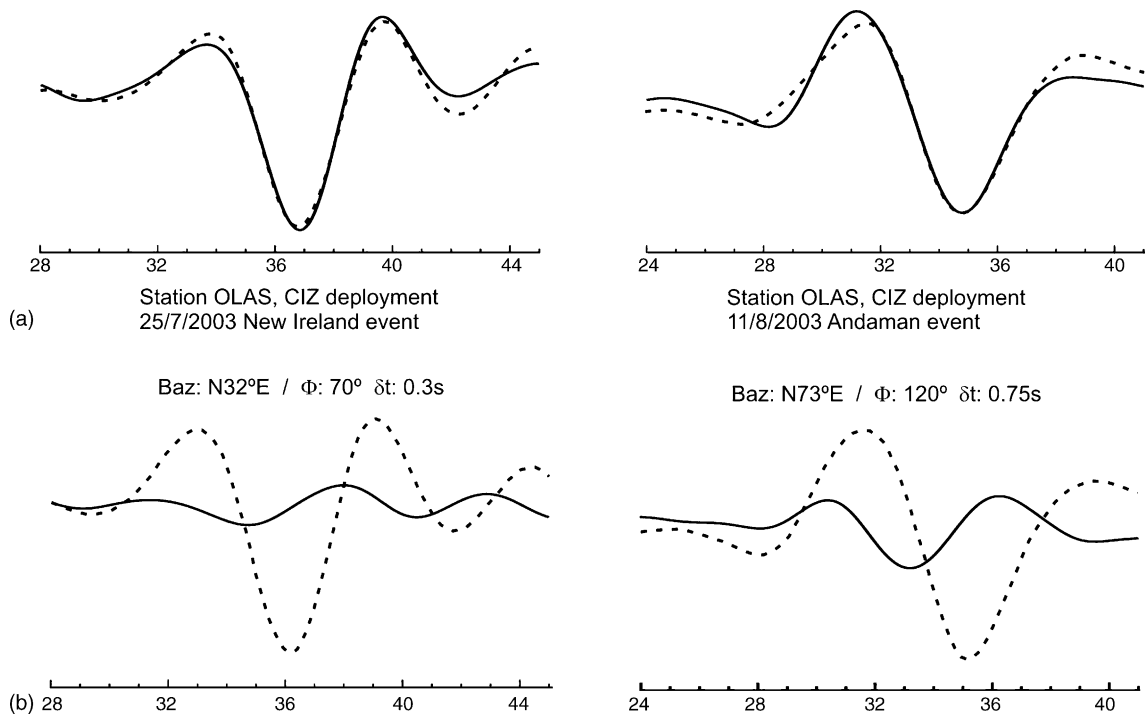


Fig. 4. Events from New Ireland Islands (left) and Andaman Islands (right) recorded at station OLAS. (a) Fitting obtained in the projections to the fast (dashed line) and slow (solid line) directions when using the values determined for by the interpretation procedure. (b) Idem when using in each event the anisotropic parameters inferred for the other event.

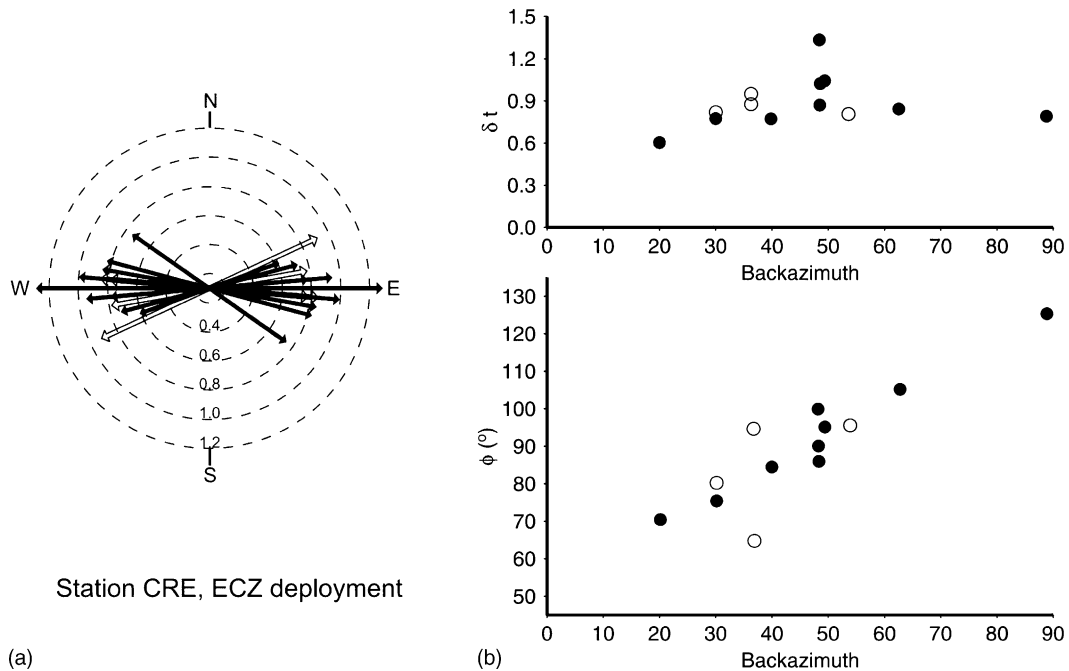


Fig. 5. (a) Measured anisotropic parameters for station CRE, at the ECZ deployment, and (b)  $\phi$  and  $\delta t$  as a function of the backazimuth of the events. Good and fair measurements are indicated using filled and open circles, respectively (see text).

shown in Fig. 5, a clear increase of  $\phi$  with backazimuth is observed, especially at the first quadrant that holds most of the available data. It is important to note that this azimuthal dependence is found in the whole investigated area, from the NW corner of Iberia to the western Pyrenees. Such dependence is not expected under the assumed hypothesis of a single layer of anisotropic material with hexagonal symmetry and horizontal symmetry axis. Local heterogeneities beneath the station could also explain the presence of some azimuthal dependence of the splitting parameters but they seem hardly compatible with the rather uniform increase of  $\phi$  with backazimuth. The fact that this dependence is observed in all the stations, located at different tectonic units, is also inconsistent with an origin related to heterogeneities. Hence, alternative models with more complex anisotropic systems, including orthorhombic symmetry, dipping axis of symmetry or multiple layers of anisotropy should be considered.

## 5. Testing alternative anisotropic models

Firstly, we explored models with a single anisotropic layer with orthorhombic symmetry and arbitrary tilt of the symmetry axis, using the ‘Splitting Modeler’ code package (Menke, 2000). We assumed an anisotropic medium consisting of 30% orthorhombic olivine and 70% isotropic olivine, a realistic mixture that is about

6% anisotropic for shear waves (Levin et al., 1999). In this case, regardless of the tilt of the symmetry axis, we obtained  $\phi$  values that remain quite close to the reference (average) value everywhere except at the singular points (every  $90^\circ$ ). This pattern clearly does not explain the progressive  $\phi$  variations observed in our case.

In the next step, we assumed the presence of two distinct anisotropic layers. In this case, the result of the propagation of a shear wave through the anisotropic media is more complex. The incident wave will split into two quasi-shear waves when propagating through the deeper anisotropic layer, and each of those wavelets will split again when entering into the second layer. Hence, the procedure to retrieve the anisotropic parameters ( $\phi$ ,  $\delta t$ ) lacks physical significance, although Silver and Savage (1994) have shown that the resulting apparent splitting parameters are meaningful quantities that display azimuthally dependent variations. If those apparent parameters could be measured along a significant azimuthal range, the anisotropic parameters of each of the layers can then be inverted.

To interpret our dataset, we use again the ‘Splitting Modeler’ package, with a model with the same mineral mixture previously described including now two anisotropic layers with orthorhombic symmetry and horizontal symmetry axis located beneath an isotropic crust. The mean value of the fast velocity direction for our whole dataset is not far from E/W. Therefore, after some

preliminary tests covering the full range of azimuths, we performed a grid search over a parameter space where the dominant layer can vary between N70E and N140E, with thicknesses ranging between 100 and 160 km, while the second layer is allowed to vary between N10W and N130E, with thicknesses ranging between 40 and 100 km. The relative position between the two layers is allowed to change. We retained the models that for each station best fit both the  $\delta t$  and  $\phi$  variations observed, especially the marked differences in  $\phi$  for events around 80° and 350° and the gently increasing slope for back-azimuths between 20° and 60°. The procedure does not provide a unique solution, but some major patterns could be constrained. For the stations located at the Central Iberian Zone and the WALZ, the best fitting model consist of an upper layer with a FVD oriented N10W and 60 km thick, over a lower layer with a N90E FVD and a

thickness of 140 km. The orientation of the dominant layer is well resolved, while that of the thin layer is loosely constrained, but lies not far from N/S. Models with similar anisotropic properties but an alternate order of the layers can provide an appropriate adjustment for the FVD but fail to fit the  $\delta t$  observations. In the eastern part of the study area, the preferred model is composed by an upper layer oriented N130E with a thickness of 100 km and a lower layer oriented N80E and 140 km thick. As for the previous case, models with similar anisotropic parameters but with a reverse sequence can not be excluded. Fig. 6 summarizes the fitting between the observed  $\phi$  and  $\delta t$  parameters and the retained model, for relevant stations along the major E–W transect covering North Iberia.

We have not explored in these retained models the influence of considering dipping layers, or different sym-

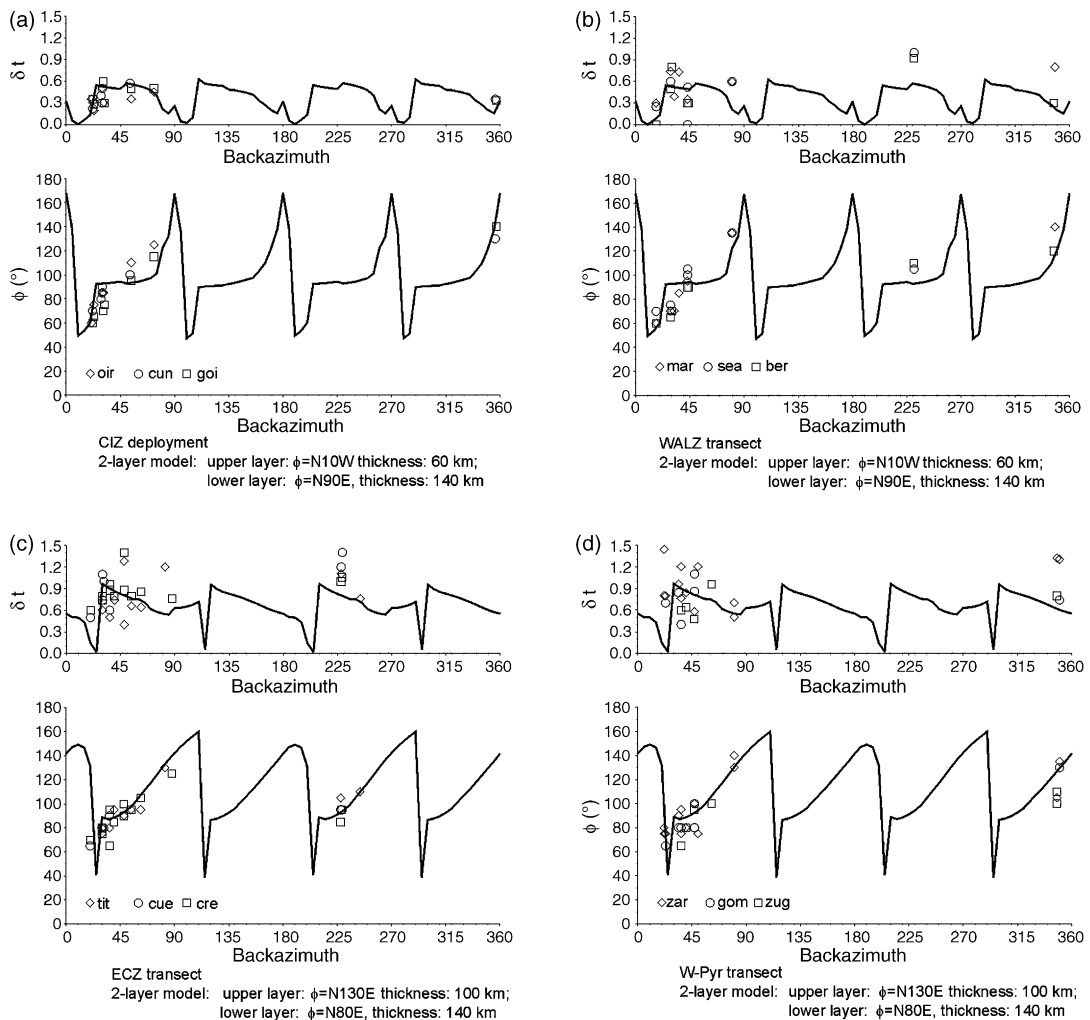


Fig. 6. Fitting between our  $\phi$  and  $\delta t$  results and those derived from the two-layer model retained for representative stations of each transect.

metry systems, because as stated by Levin et al. (1999) differences between orthorhombic and hexagonal models, as well as the variations induced by tilting of the symmetry axis are only significant nearby the discontinuity points. Hence, extensive back-azimuth coverage is needed to try to discern between them.

## 6. Discussion

The most consistent elements of our retained models are the presence of two anisotropic layers of different thicknesses. The lower level layer, with a FVD oriented close to E/W throughout the northern part of Iberia, is the most prominent one. The upper level layer is thinner and its properties vary between the eastern and western sections of the transect, explaining the differences observed in  $\delta t$ .

The dominant E/W anisotropic layer is unlikely to be associated to asthenospheric dynamic flow related to present-day absolute plate motion (APM) of Eurasia. The HS3-NUVEL1A model (Gripp and Gordon, 2002), predicts a slow plate velocity of 1.9 cm/year with a rough NE–SW direction, significantly different from the dominant FVD observed.

On the other hand, this E–W dominant layer could be interpreted as ‘frozen-in’ anisotropy in the lower lithosphere, related to the most relevant orogenic process in the area. In the western Pyrenees and the Cantabrian Mountains a similar E–W structural direction may arise from either Variscan or Alpine tectonic episodes (Barruol et al., 1998; Díaz et al., 2002). Results obtained at stations located at the central, axial zones greatly affected by the Alpine compression are very similar to those derived from stations located at more external domains, much less involved in this orogeny. This fact seems to favor the explanation of the dominant anisotropic direction as a signature of the widespread Variscan tectonics in North Iberia. However, if this Variscan hypothesis is assumed, then the expected dominant anisotropic direction at the WALZ and at the Central Iberian Zone in Galicia should be N/S, according to their dominant tectonic lineaments. However, our new results show again E/W fast velocity directions at those tectonic domains, as for the previous transects eastwards, and therefore make unlikely this Variscan explanation.

Alternatively to prominent anisotropy being related to Variscan or Alpine compressional events, the large-scale Mesozoic extensional event in-between could be at the origin of the E/W anisotropy layer found throughout the northern Iberian Peninsula. The opening of North Atlantic Ocean and Bay of Biscay resulted in dominant spreading directions oriented roughly E/W

and N/S, respectively (Sibuet et al., 2004). During the Cretaceous, this extensional episode generated a left-lateral shift of Iberia with respect to Eurasia. The extent of this deformation varies in the different geodynamic models considered (Olivet, 1996; Rosenbaum et al., 2002; Srivastava et al., 1990), but in any case it constitutes a major transtensional regime and, as such, may have led to a significant anisotropic imprint around the lithosphere–asthenosphere transition. A similar explanation has been proposed by Barruol et al. (2004) to account for the anisotropy observations in SE of France, which they relate to the lateral, extensional movements of the Corsica-Sardinia block. The overall E/W fast velocity direction observed throughout North Iberia could therefore be related to the displacement of the Iberian plate due to the extensional processes in the North Atlantic and Bay of Biscay domains. Such kind of anisotropy is compatible with other SKS splitting results previously obtained in the Iberian Peninsula. Díaz et al. (1998), using data from the NARS temporary array deployed over Iberia, reported FVD directions oriented roughly E/W at sites covering the Iberian Massif of center Iberia. More recently, Schmid et al. (2002), in a compilation of shear-wave splitting results in the Mediterranean region, reported also FVD directions for permanent stations at the Central Iberian Zone. Their results are located S of the region here investigated, with a mean direction close to E/W, showing, as in our work, a significant spread in the results. They explained this anisotropy by a simple asthenospheric flow model. Barruol et al. (1998) reported a mean  $\phi = N100^\circ E$  and  $\delta t = 1.5$  s throughout the whole Pyrenean belt. Their results are consistent with the measurements here presented and allow to extend the northern Iberia transect to the Mediterranean Sea. In their interpretation, the anisotropy was associated to the imprint of the Hercynian and Alpine tectonics, both with a similar E/W orientation in that area, and therefore hard to be differentiated by SKS splitting.

Our two-layered models include an isotropic crust over the anisotropic lithospheric layers. At present we cannot exclude the presence of crustal anisotropy that would in that case overprint the contribution of the weaker anisotropic layer. Additional constraints could be provided by an analysis of receiver function data in terms of anisotropy we expect to develop in the near future. However, such possible crustal contribution would have a more minor effect than our modeled weaker anisotropy layer and, therefore, a subcrustal anisotropy level is still required to explain the data. This layer can be interpreted as a signature of the major orogenic processes, and the differences in FVD inferred between the western data set (N10W) and the eastern one (N130E) could

be attributed to the Variscan directions in the hinterland part of the Variscan Belt, and to the Variscan plus Alpine directions in the Cantabrian Mountains and Pyrenees.

## 7. Conclusions

Seismic anisotropy has been evidenced from shear-wave splitting analysis throughout the Northern part of the Iberian Peninsula, from the western Pyrenees to the most hinterland parts of the Variscan belt, showing consistently an average fast velocity direction close to E–W. Delay times up to 1.5 s are observed in most transects, but lower values, not exceeding 1 s are measured at the westernmost part, in the Iberian Massif.

Additionally, an azimuthal dependence of the splitting parameters is also well established, denoting a complex distribution at depth of the anisotropic features. The observations are not supported by considering single-layer models, either with hexagonal or orthorhombic symmetry systems, and/or dipping axes of symmetry. Two-layer anisotropic models with an orthorhombic symmetry system explain satisfactorily the observed patterns both in the  $\phi$ /backazimuth variation and in the overall  $\delta t$  values, even if some of the anisotropic parameters are loosely constrained from the available data set.

In all the retained models the two layers exhibit different thicknesses. The most prominent contribution to the observed anisotropy comes from a layer consistently oriented close to E/W, whereas the thinner second layer ‘modulates’ the result. The fast direction of the latter has been interpreted to change along the transect, which may account for the differences in  $\delta t$  observed between the eastern and western part of the study area. The relative position of these two layers is not fully constrained but models with dominant anisotropy at the lower level seem to provide an enhanced fitting.

The previous anisotropy measurements in the northern part of Iberia were limited to the Pyrenean belt (Barruol et al., 1998), where it is difficult to establish the origin of the anisotropy, as the Hercynian and Alpine structures, as well as the dominant extensional direction have a roughly parallel E–W trend. In this study we have shown that the Hercynian orogeny cannot be the main deformation event responsible for the anisotropy observed in northern Iberia, as the mean FVD measured at the CIZ is far from the N/S direction of the Hercynian structures in this zone. The dominant E–W anisotropic layer throughout North Iberia may correspond to an anisotropic imprint around the lithosphere–asthenosphere transition related to the eastward displacement of the Iberian plate due to the Mesozoic extensional processes in the North Atlantic and Bay

of Biscay domains. The weaker anisotropic layer on top could likely be associated to an additional anisotropic signature within the lithosphere led by major Variscan and Alpine orogenic processes, with a possible minor contribution of crustal anisotropy.

## Acknowledgments

This work was sponsored by Spanish Research Ministry projects AMB98-1012-C02 and REN2001-1734-C03. M. Ruiz and C. López benefits from PhD F.P.I. grants. Additional support is provided by the Dep. of Universities, Research and Society of the Generalitat de Catalunya government. The authors are members of the team Consolider-Ingénio 2010 CSD2006-00041.

## References

- Alonso, J.L., Pulgar, J.A., García-Ramos, J.C., Barba, P., 1996. Tertiary basins and alpine tectonics in the cantabrian mountains (NW Spain) in tertiary basins of Spain, in: Friend, P.F., Dabrio, C.J., (Eds.), *The stratigraphic record of crustal kinematics*, Cambridge University Press, Cambridge, pp. 214–227.
- Barruol, G., Mainprice, D., 1993. A quantitative evaluation of crustal rocks to the shear-wave splitting of teleseismic SKS waves. *Phys. Earth Planet. Interiors* 78, 281–300.
- Barruol, G., Souriau, A., Vauchez, A., Díaz, J., Gallart, J., Tubia, J., Cuevas, J., 1998. Lithospheric anisotropy beneath the Pyrenees from shear wave splitting. *J. Geophys. Res.* 103, 30039–30054.
- Barruol, G., Deschamps, A., Coutant, O., 2004. Mapping upper mantle anisotropy beneath SE France by SKS splitting indicates Neogene asthenospheric flow induced by Apenninic slab roll-back and deflected by the deep Alpine roots. *Tectonophysics* 394, 125–138.
- Choukroune, P., The ECORS-Pyrenees-Team, 1989. The ECORS Pyrenean deep seismic profile reflection data and the overall structure of an orogenic belt. *Tectonics* 8 (1), 23–39.
- Crampin, S., 1981. A review of wave motion in anisotropic and cracked elastic-media. *Wave Motion* 3, 343–391.
- Díaz, J., Gallart, J., Ruiz, M., Pulgar, J.A., López, C., González-Cortina, J.M., 2002. Anisotropic features of the Alpine Lithosphere in Northern Spain. *Geophys. Res. Lett.* 29 (24), doi:10.1029/2002GL015997.
- Díaz, J., Gallart, J., Pedreira, D., Pulgar, J.A., Ruiz, M., Lopez, C., González-Cortina, J.M., 2003. Teleseismic probing of alpine crustal thickening and wedging beneath the cantabrian mountains and western Pyrenees. *Geophys. Res. Lett.* 30, doi:10.1029/2003GL017073.
- Díaz, J., Gallart, J., Hirn, A., Paulssen, H., 1998. Anisotropy beneath the Iberian Peninsula: the contribution of the ILIHA-NARS broadband experiment. *Pageoph* 151, 395–405.
- Farías, P., Gallastegui, G., González-Lodeiro, F., Marquínez, J., Martín-Parra, L.M., Martínez-Catalán, J.R., Pablo Maciá, J.G., Rodríguez Fernández, R., 1987. Aportaciones al conocimiento de la litoestratigrafía y estructura de Galicia Central. *Mem. Fac. Cienc. Porto* 1, 411–431.
- Gallastegui, J., Pulgar, J.A., Gallart, J., 2002. Initiation of an active margin at North Iberian continent-ocean transition. *Tectonics* 21, doi:10.1029/2001TC901046.

- Gripp, A.E., Gordon, R.G., 2002. Young tracks of hotspots and current plate velocities. *Geophys. J. Int.* 150, 321–361.
- Julivert, M., Fontboté, J.M., Ribeiro, A., Conde, L., 1972. Mapa Tectónico de la Península Ibérica y Baleares, 1:1.000.000. Inst. Geol. Min. Esp. Madrid, 113.
- Julivert, M., Martínez, F., Ribeiro, A., 1980. The Iberian segment of the European Hercynian Fol. Belt. In: Proceedings of the 26th Congr. Geol. Int., Paris 1980. Colloq. C6, Géologie de l'Europe, du Précambrien aux bassins sédimentaires posthercyniens. *Bur. Rech. Geol. Min. Mém.* 108, 132–158.
- Levin, V., Menke, W., Park, J., 1999. Shear wave splitting in the Appalachians and the Urals: a case for multilayered anisotropy. *J. Geophys. Res.* 104, 17975–17993.
- López-Fernández, C., Pulgar, J.A., Gallart, J., González-Cortina, J.M., Díaz, J., Ruíz, M., 2004. Sismicidad y tectónica en el área de Becerreá—Triacastela (Lugo, NO España). *Geogaceta* 36.
- Mainprice, D., Nicolas, A., 1989. Development of shape and lattice preferred orientations: application to the seismic anisotropy of the lower crust. *J. Struct. Geol.* 11 (1/2), 175–189.
- Martínez Catalán, J.R., Pérez-Estaún, A., Bastida, F., Pulgar, J.A., Marcos, A., 1990. West Asturian-Leonese zone: structure. In: Dallmeyer, R.D., Martínez, E. (Eds.), *Pre-Mesozoic Geology of Iberia*. Springer-Verlag, Berlin, pp. 103–114.
- Matte, Ph., 1986. Tectonics and plate tectonics model for the Variscan belt of Europe. *Tectonophysics* 126, 329–374.
- Matte, Ph., 1991. Accretionary history and crustal evolution of the Variscan belt in Western Europe. *Tectonophysics* 196, 309–337.
- Menke, W., 2000. SPLITTING MODELER Software. [ftp://ftp.ldeo.columbia.edu/pub/menke/SPLITTING\\_MODELER.tar.Z](ftp://ftp.ldeo.columbia.edu/pub/menke/SPLITTING_MODELER.tar.Z).
- Muñoz, J.A., 1992. Evolution of a continental collision belt: ECORS-Pyrenees crustal balanced cross section. In: McClay, K. (Ed.), *Thrust Tectonics*. Chapman and Hall, New York, pp. 235–246.
- Nicolas, A., Christensen, N.I., 1987. Formation of anisotropy in upper mantle peridotites. A review. In: Fuchs, K., Froidevaux, C. (Eds.), *Composition, Structure and Dynamics of the Lithosphere–Asthenosphere System*. AGU, Washington, pp. 137–154.
- Olivet, J.-L., 1996. La cinématique de la plaque Ibérie. *Bull. Cent. Rech. Explor.-Prod. Elf Aquitaine* 20, 131–195.
- Park, J., Levin, V., 2002. Seismic anisotropy: tracing plate dynamics in the mantle. *Science* 296, 485–489.
- Pedreira, D., Pulgar, J.A., Gallart, J., Díaz, J., 2003. Seismic evidence of Alpine crustal thickening and wedging from the Western Pyrenees to the Cantabrian Mountains (North Iberia). *J. Geophys. Res.* 108 (2004), doi:10.1029/2001JB001667.
- Pérez-Estaún, A., Bastida, F., Alonso, J.L., Marquínez, J., Aller, J., Álvarez-Marrón, J., Marcos, A., Pulgar, J.A., 1988. A thin-skinned tectonics model for an arcuate Fol. and thrust belt: the Cantabrian Zone (Variscan Ibero-Armorican Arc). *Tectonics* 7, 517–537.
- Pérez-Estaún, A., Pulgar, J.A., Banda, E., Álvarez-Marrón, J., ESCIN Research Group, 1994. Crustal structure of the external variscides in northwest Spain from deep seismic reflection profiling. *Tectonophysics* 232, 91–118.
- Rosenbaum, G., Lister, G.S., Duboz, C., 2002. Relative motions of Africa, Iberia and Europe during Alpine orogeny. *Tectonophysics* 359, 117–129.
- Ruiz, M., Gallart, J., Díaz, J., Olivera, C., Lopez, C., González-Cortina, J.M., Pulgar, J.A., 2006a. Seismic activity in the Western Pyrenean edge. *Tectonophysics* 412 (3–4), 217–235, doi:10.1016/j.tecto.2005.10.034.
- Ruiz, M., Díaz, J., Gallart, J., González-Cortina, J.M., Pulgar, J.A., 2006b. Seismotectonic constraints at the western edge of the Pyrenees: aftershock series monitoring of the 2002 February 21, 4.1 Lg earthquake. *Geophys. J. Int.* 166 (1), 238–252, doi:10.1111/j.1365-246X.2006.02965.x.
- Savage, M.K., 1999. Seismic anisotropy and mantle deformation: what have we learned from shear wave splitting? *Rev. Geophys.* 37, 65–106.
- Schmid, Ch., van der Lee, S., Giardini, D., 2002. Delay times and shear wave splitting in the Mediterranean region. *Geophys. J. Int.* 159, 275–290.
- Séguret, M., Daignières, M., 1986. Crustal scale balanced cross-sections of the Pyrenees; discussion. *Tectonophysics* 129, 303–318.
- Sibuet, J.-Cl., Srivastava, S.P., Spakman, W., 2004. Pyrenean orogeny and plate kinematics. *J. Geophys. Res.* 109, B08104, doi:10.1029/2003JB002514.
- Silver, P.G., Savage, M.K., 1994. The interpretation of shear-wave splitting parameters in the presence of two anisotropic layers. *Geophys. J. Int.* 119, 949–963.
- Srivastava, S.P., Schouten, H., Roest, W.R., Klitgord, K.D., Kovacs, L.C., Verhoef, J., Macnab, R., 1990. Iberian plate kinematics: a jumping boundary between Eurasia and Africa. *Nature* 344, 756–759.
- Teixell, A., 1998. Crustal structure and orogenic material budget in best central Pyrenees. *Tectonics* 17, 395–406.
- Vergés, J., Millán, H., Roca, E., Muñoz, J.A., Marzo, M., Cirés, J., Den Bezemer, T., Zoetemeijer, R., Cloetingh, S., 1995. Eastern Pyrenees and related foreland basins: Pre-, syn- and post-collisional crustal-scale cross-sections. *Mar. Pet. Geol.* 12, 893–915.